Effect of surface wettability on liquid density, structure, and diffusion near a solid surface

J. A. Thomas and A. J. H. McGaughey[a)]
Department of Mechanical Engineering, Carnegie Mellon University, Pittsburgh, Pennsylvania 15213

(Received 5 October 2006; accepted 27 November 2006; published online 19 January 2007)

Molecular dynamics and Langevin dynamics simulations are used to elucidate the behavior of liquid atoms near a solid boundary. Correlations between the surface wettability and spatial variations in liquid density and structure are identified. The self-diffusion coefficient tensor is predicted, revealing highly anisotropic and spatially varying mass transfer phenomena near the solid boundary. This behavior affects self-diffusion at a range of time scales. Near a more-wetting surface, self-diffusion is impeded by strong solid-liquid interactions that induce sharp liquid density gradients and enhanced liquid structure. Conversely, near a less-wetting surface, where solid-liquid interactions are weaker, the liquid density is low, the atoms are disordered, and diffusion is enhanced. These findings suggest that altering the wettability of a micro- or nanochannel may provide a passive means for controlling the diffusion of select targets towards a functionalized surface and controlling the reaction rate in diffusion-limited reactions. © *2007 American Institute of Physics*. [DOI: 10.1063/1.2424934]

I. INTRODUCTION

Molecular behavior near material and phase boundaries is complex and difficult to predict. Near an interface (the boundary region separating two fluid domains[1]), molecules follow phase diagrams and thermodynamic functions different from either bulk phase.[2] Near a surface (the region around a solid-solid or solid-liquid boundary), molecular behavior is governed by interactions between the two different materials.[1,3] The sharp gradients in properties near boundaries are generalized in a continuum-level analysis by using mathematically convenient boundary conditions (e.g., assumptions of no slip, continuous temperature profiles, and continuous concentration profiles). As the scale of engineering systems transitions to the nanoscale, the atomic-level behavior near boundaries assumes a larger role in the overall system behavior.[4–7] Continuum-based boundary conditions may not be applicable to nanoscale analysis, and an understanding of the actual atomic behavior near surfaces and interfaces is required.

Near a solid-liquid boundary, spatially varying properties are prevalent and have been correlated to the surface wettability.[8–11] Surface wettability is a measure of the relative strengths of the solid-liquid and liquid-liquid interactions, and is manifest in the contact angle that forms between a liquid droplet and a solid.[1] When liquid atoms experience significant attraction to the surface, the contact angle is less than 90° and the surface is said to be wetting. When liquid dynamics are dominated by liquid-liquid interaction, the contact angle is greater or equal to 90° and the surface is said to be nonwetting.[12] While the notion of a contact angle is not applicable to liquids confined in micro- or nanochannels, the relationships between wettability, solid-liquid interaction strength, and spatially varying liquid properties are still valid.

Efforts have been made to vary surface wettability to generate tailored transport properties within micro- and nanoscale solid-liquid systems. Hendy *et al.*,[13] using a model based on the Navier-Stokes equation, analytically demonstrated that patterned surface wettability and the associated variations in slip length can induce complex mixing patterns in microfluidic devices. Similarly, Kuksenok *et al.*[14] and Kuksenok and Balazs[15] used a lattice Boltzmann model for fluid dynamics to show that surface patterning can be exploited to control the flow and mixing of binary fluids. Using molecular dynamics (MD) simulations, Barrat and Chiaruttini[5] demonstrated that tailored thermal resistance across a liquid-solid boundary can be obtained by tuning the strength of the solid-liquid interactions.

To complement these investigations and to further understand atomic transport near a solid-liquid boundary, we investigate the self-diffusion of liquid atoms near solid surfaces of different wettability. We begin by using MD simulations to predict and compare the density and structure of liquid atoms near more- and less-wetting solid surfaces. Next, by tracking the atomic positions, we predict survival probabilities, exit probabilities, and atomic mean-squared displacements. We augment the MD data with predictions from Langevin dynamics simulations and identify the spatial dependence of the anisotropic self-diffusion coefficient tensor. Using these findings we present a mechanistic description of liquid self-diffusion (hereto called diffusion) occurring over a range of time scales.

[a)]Author to whom correspondence should be addressed. Electronic mail: mcgaughey@cmu.edu

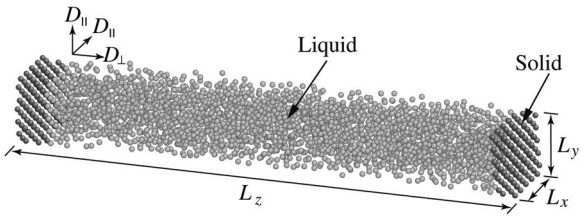

FIG. 1. Simulation cell used to model a solid-liquid boundary. The configuration consists of 2900 atoms with periodic boundary conditions imposed in all three directions. The wide channel generates two independent solid-liquid boundaries.

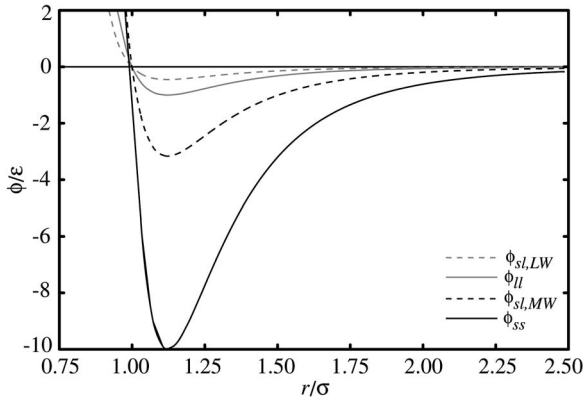

FIG. 2. Comparison between the solid-solid, liquid-liquid, and solid-liquid interaction energies. Interaction strength is a function of distance and is proportional to $\epsilon_{\alpha\beta}$ [see Eq. (1)]. The solid-solid and liquid-liquid interactions in both the more-wetting (MW) and less-wetting (LW) simulations are identical.

II. SIMULATION SETUP AND TIME SCALE CONSIDERATIONS

A. Molecular dynamics simulations

The small length and time scales associated with atomic-level dynamics limit the ability of laboratory experiments to resolve nanoscale transport phenomena. Instead, MD simulations, which can access these scales, have become a common tool for modeling atomistic transport.[16–19] Molecular dynamics is a simulation technique that uses Newton's laws of motion to predict the position and momenta space trajectories of a system of classical particles. The only required inputs are an interatomic potential, which is used to calculate potential energies and forces, and an initial atomic configuration.

The Lennard-Jones (LJ) interatomic pair potential is commonly used in MD simulations of solid-liquid boundaries.[5,13,20,21] This simple potential allows for the identification of phenomena that may be difficult to resolve in simulations of more complicated materials. For a multicomponent system, the LJ potential can be written as

$$\phi_{\alpha\beta}(r_{ij}) = 4\epsilon_{\alpha\beta}\left[\left(\frac{\sigma_{\alpha\beta}}{r_{ij}}\right)^{12} - \left(\frac{\sigma_{\alpha\beta}}{r_{ij}}\right)^{6}\right], \quad (1)$$

where r_{ij} is the distance between atoms i and j, ϵ is the depth of the interaction energy well, and $2^{1/6}\sigma$ is the equilibrium pair separation distance. The subscripts α and β are used to distinguish the interactions between different species.

The MD simulation cell we use to model a solid-liquid boundary is shown in Fig. 1. It contains 2450 liquid atoms and 450 solid atoms with periodic boundary conditions imposed in all three directions. We take the liquid to be argon with $\epsilon_{ll}=1.67\times10^{-21}$ J and $\sigma_{ll}=3.4\times10^{-10}$ m.[22] As in previous work on LJ solid-liquid systems, the channel walls are a generic solid modeled with $\epsilon_{ss}=10\epsilon_{ll}=10\epsilon$ and $\sigma_{ss}=\sigma_{ll}=\sigma$.[21] The solid atoms are arranged into a face-centered-cubic (fcc) crystal with 5 unit cells in the x and y directions and 4.5 unit cells in the z direction. The noninteger number of unit cells in the z direction generates a midplane where two atoms are fixed at their equilibrium positions to prevent the solid phase from drifting.

The surface wettability is tuned by adjusting the solid-liquid parameter ϵ_{sl}. As shown in Fig. 2, where all the potential energy curves used are plotted, setting ϵ_{sl} to a value greater than 1 makes the solid-liquid interaction stronger than the liquid-liquid interaction (increasing the surface wettability) and setting ϵ_{sl} to a value less than 1 has the opposite effect. In line with other investigations, a more-wetting surface is modeled by setting ϵ_{sl} to $\sqrt{10}\epsilon$.[21] To model a less-wetting surface, we select an ϵ_{sl} value of 0.45ϵ. In simulations of a liquid droplet in contact with a solid surface, these wetting parameters generate contact angles of approximately 0° (more-wetting) and 85° (less-wetting).[12]

Data are collected from MD simulations run in the *NVE* (constant mass, volume, and energy) ensemble. The simulations are performed at a temperature of 90 K, above the argon melting temperature of 83.8 K. The equations of motion are integrated using the Verlet leapfrog scheme with a 4.285 fs time step. All interactions are subject to a continuous force/continous energy cutoff radius of 2.5σ.

The bulk solid zero-pressure lattice constant is 1.552σ. In the simulation cell, the pressure of the liquid atoms on the solid atoms is weaker than that within the solid. This discrepancy causes the lattice constant perpendicular to the solid-liquid surface to naturally be slightly larger than the lattice constant parallel to the surface. We generate an isotropic lattice constant by increasing the parallel-to-surface simulation cell dimensions (L_x and L_y) to 7.830σ, corresponding to a solid lattice constant of 1.566σ.

The 90 K zero-pressure density of the bulk liquid (ρ_0, obtained from liquid-only simulations) is 1170 kg/m^3. To ensure that the two surfaces are isolated, we require that the liquid obtain a uniform density of ρ_0 away from the solid surface and maintain this density across the channel centerline. For the more-wetting and less-wetting conditions, we satisfy this condition using L_z values of of 63.7σ and 65.7σ, corresponding to channel widths of 15.1 and 15.7 nm. Adjusting L_z has no significant effect on the boundary region density profile.

For analysis purposes, the region inside the channel is virtually partitioned into 0.785σ intervals (one-half of the solid lattice constant) to form a sequence of equal-volume layers parallel to the channel walls. This spatial discretization allows for a direct investigation of the effects of the solid on the behavior of the liquid at various distances from the surface. The implementation of this layering scheme has no influence on the liquid dynamics.

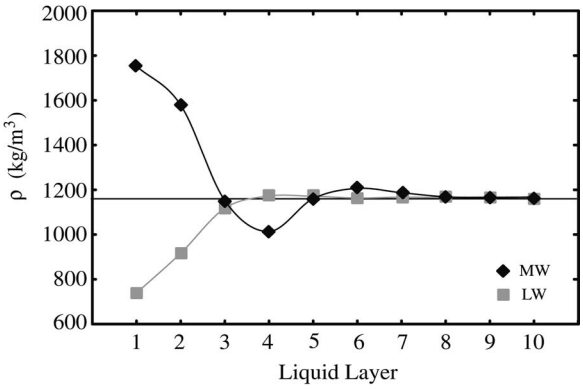

FIG. 3. Density profiles near the more-wetting and less-wetting solids. Guidelines are added to highlight the local minima and maxima. The bulk liquid density (ρ_0, horizontal line) is recovered in layers far from the solid surface and continues across the channel centerline. Each liquid layer is 0.267 nm (0.785σ) thick.

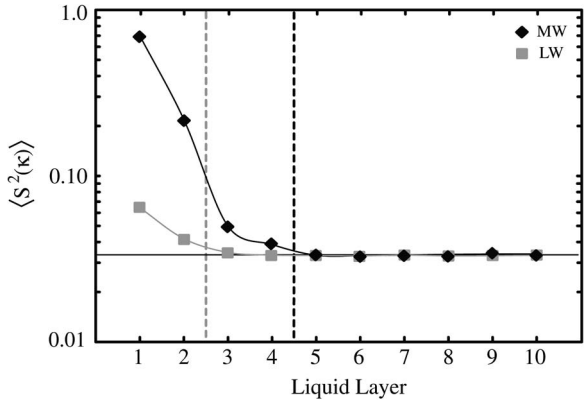

FIG. 4. The liquid structure factor $\langle S^2(\boldsymbol{\kappa})\rangle$ near the more-wetting and less-wetting surfaces. The solid horizontal line indicates the bulk liquid structure. Near the more- and less-wetting solid, $\langle S^2(\boldsymbol{\kappa})\rangle$ equals the bulk value in layers 5 and 3, respectively. The dashed lines represent the boundary between solid-moderated and liquid-moderated regions.

B. Atomic diffusion versus atomic migration

As predicted by classical mechanics, the mean-squared displacement (MSD) of a diffusing fluid particle is initially quadratic with respect to time.[23] The curvature of the MSD is important when calculating short-time dynamical quantities such as the memory kernel or velocity autocorrelation function.[23] At longer times, as the statistical nature of the atomic interactions takes over, the MSD becomes linear with a slope proportional to the diffusion coefficient.[24] From simulations of bulk liquid argon, we predict that this transition from a quadratic to a linear MSD occurs after 0.21 ps of particle tracking. This result is in good agreement with the transition time predicted by Rahman,[25] who performed similar liquid argon simulations.

All mass transport in our system is diffusive. For the purposes of discussion, we make a distinction between atomic diffusion and atomic migration. We use the term atomic diffusion to describe the transport of atoms *within* each liquid layer over a period of 21 ps. This duration is long enough to ensure that our measurements are dominated by a MSD linearly dependent on time, but short enough to ensure that liquid atoms remain in a single layer long enough to measure local mass transfer properties. We use the term "atomic migration" to describe the transport of atoms *across* several layers over a period of 420 ps. These long trials allow us to investigate the behavior of atoms as they exit a layer and disperse throughout the system.

III. DATA COLLECTION AND RESULTS

A. Density profiles

Although the liquid atoms are continually moving, the time-averaged number of atoms in each liquid layer j is well defined. Close to the surface, this mean layer density ρ_j varies as a function of the distance from the solid. Far from the surface, where bulk statistics are recovered, the average number of atoms in each layer is spatially uniform and corresponds to the bulk density. As shown in Fig. 3, the layer-specific densities and the shape of the resulting density profile are strong functions of surface wettability. The layer-specific data presented here and throughout this report were obtained by averaging between both solid-liquid boundaries over four data sets, each consisting of 150 independent 21 ps trials. Error bars in all subsequent figures indicate the range of values generated by the four data sets. For many points the error bars are smaller than the data markers.

B. Planar structure factor

The square of the planar structure factor, $\langle S^2(\boldsymbol{\kappa})\rangle$, was introduced by Lutsko *et al.*[26] as a means to quantify the breakdown of crystalline order during melting. The same formulation has been applied by Xue *et al.*[21] to a confined liquid to measure the layer-by-layer breakdown of liquid ordering near a solid surface. Within liquid layer j, $\langle S_j^2(\boldsymbol{\kappa})\rangle$ is given by

$$\langle S_j^2(\boldsymbol{\kappa})\rangle = \left[\frac{1}{N_j}\sum_i \cos(\boldsymbol{\kappa}\cdot\mathbf{q}_i)\right]^2 + \left[\frac{1}{N_j}\sum_i \sin(\boldsymbol{\kappa}\cdot\mathbf{q}_i)\right]^2, \tag{2}$$

where $\mathbf{q}_i$ is the planar position (x,y) of atom i, N_j is the number of atoms in layer j, and $\boldsymbol{\kappa}$ is a reciprocal space lattice vector. The summations are taken over all atoms in layer j. When applied to a perfect crystal at zero temperature, $\langle S^2(\boldsymbol{\kappa})\rangle$ is unity. When applied to a system with noninteracting particles (e.g., an ideal gas), $\langle S^2(\boldsymbol{\kappa})\rangle$ is zero.

Near the channel walls, the liquid assumes a structure similar to the solid so that $\boldsymbol{\kappa}$ is taken to be $2\pi/a(\hat{\boldsymbol{i}}+\hat{\boldsymbol{j}})$, where a is the fcc crystal lattice constant. A plot of the structure factor for the ten layers closest to the solid walls for both wettabilities is presented in Fig. 4. The magnitude of $\langle S^2(\boldsymbol{\kappa})\rangle$ agrees well with the results of Xue *et al.*,[21] who applied Eq. (2) to a similar more-wetting condition.

Near the more-wetting and less-wetting surfaces, the predicted structure profiles suggest a natural division between regions in which the liquid dynamics are moderated by interactions with the solid and regions in which the liquid dynamics are moderated by interactions with other liquid atoms. These divisions are shown in Fig. 4. In the solid-moderated region, consisting of layers 1–4 in the more-wetting simulation and layers 1 and 2 in the less-wetting simulation, $\langle S_j^2(\boldsymbol{\kappa})\rangle$ is greater than the bulk liquid value. In

the liquid-moderated region, which consists of all other liquid layers, $\langle S_j^2(\boldsymbol{\kappa})\rangle$ is equivalent to the bulk value. Although the imposed 2.5σ cutoff radius prevents direct solid-liquid interactions beyond layer 3, we found that increasing the cutoff to 3.5σ had no significant effect on the shape and magnitude of the predicted density and structure profiles.

C. Survival probability curves and exit probabilities

During tracking, the atoms originally comprising a liquid layer gradually exit into neighboring layers. This behavior generates a time-dependent ratio between the numbers of atoms that originate and remain in a given layer, known as the survival probability P. The time dependence of P is the survival probability curve,[27] which for liquid layer j is given by

$$P_j(\tau) = \frac{N_j(\tau)}{N_j(0)}, \tag{3}$$

where τ is time, $N_j(0)$ is the number of atoms in the liquid layer at $\tau=0$, and $N_j(\tau)$ is the number of original atoms remaining in the layer at time τ. Atoms that leave and reenter the layer are not considered in $N_j(\tau)$. We observe that the survival curve decays according to $P_j(\tau) \simeq e^{-\tau/\tau_j}$. The layer-specific decay constant τ_j is 2.80 ps in bulklike layers and varies between 1.70 and 3.03 ps in layers closer to the solid where there is diffusion.

Throughout a trial we record both the number of atoms in a given layer that exit towards the solid surface and the number of atoms that exit towards the channel centerline. We then divide these values by $N_j(0)$ to predict layer-specific solid-side exit probabilities $P_{j,s}$ and centerline-side exit probabilities $P_{j,c}$. In the bulklike layers far from either surface, the movement of the atoms is unbiased and $P_s=P_c=0.5$. Closer to the surface, P_s and P_c become unequal as solid interactions and liquid density variations influence atomic dynamics.

D. Atomic diffusion

1. Isotropic versus anisotropic diffusion

In a MD simulation, the diffusion coefficient D_0 of an isotropic system is typically predicted using either the Green-Kubo method or the Einstein method. When using the Green-Kubo method, D_0 is found from the integral of the velocity autocorrelation function.[28] In the Einstein method, D_0 of a three-dimensional system is predicted from the MSD of tracked particles by

$$D_0 = \frac{\sum_{i=1}^{N} \langle |\mathbf{r}_i(\tau) - \mathbf{r}_{i,0}|^2 \rangle}{6N\tau}, \tag{4}$$

where N is the number of atoms in the simulation, $\mathbf{r}_0$ is the initial position (x,y,z) of atom i, and $\mathbf{r}(\tau)$ its position at time τ.[24] The Einstein relation is valid only after the MSD has become linearly dependent on time (see Sec. II). Recognizing this fact, we use Eq. (4) to predict a bulk diffusion coefficient of 4.03×10^{-9} m^2/s from liquid-only simulations.

When using either the Green-Kubo or Einstein methods to evaluate D_0, it is assumed that the diffusing atoms travel without directional bias and evenly sample the simulation space. However, when modeling transport near surfaces, interfaces, or other systems with spatial gradients, these diffusion formulations are not valid.[1,11,27,29] The diffusion coefficient becomes directionally dependent (i.e., anisotropic) and must be replaced by the diffusion coefficient tensor, describing diffusion parallel ($D_\parallel$) and perpendicular ($D_\perp$) to the solid surface. Liu *et al.*[27] and Wick and Dang[29] have developed techniques to predict the diffusion coefficient tensor near a liquid-vapor interface. The approach of Wick and Dang is applied here to the solid-liquid boundary.

2. Diffusion parallel to the surface

Within each liquid layer, the diffusion coefficient parallel to the solid surface, $D_{j,\parallel}$, is found using a modified form of the Einstein method,[27,29]

$$D_{j,\parallel} = \lim_{\tau\to\infty} \frac{\langle [\Delta q(\tau)]^2 \rangle_{\mathbf{R}_j}}{4\tau P_j(\tau)}. \tag{5}$$

The numerator within the argument of the limit is the average MSD of liquid atoms that remain in the layer at each time step and is found from

$$\langle [\Delta q(\tau)]^2 \rangle_{\mathbf{R}_j} = \frac{1}{N_j(0)} \sum_{i\in\mathbf{R}_j} [\mathbf{q}_i(\tau) - \mathbf{q}_i(0)]^2, \tag{6}$$

where $\mathbf{R}_j=\mathbf{R}_j(\tau)$ is the subset of the original liquid atoms that remain in layer j at time τ, $\mathbf{q}_i(\tau)$ is the planar position of each atom within the subset $\mathbf{R}_j$, and $\mathbf{q}_i(0)$ is the initial position of each atom. To account for atoms that exit the layer, $\langle [\Delta q(\tau)]^2 \rangle_{\mathbf{R}_j}$ must be scaled by the survival probability $P_j(\tau)$ at each time step.[27,29]

As τ increases, $\mathbf{R}_j$ tends towards the null set and the sample size used to evaluate $D_{j,\parallel}$ becomes smaller. To evaluate $D_{j,\parallel}$ while minimizing the noise associated with such small data sets, the argument of the limit in Eq. (5) is averaged over the final 250 time steps (1.1 ps) where $\mathbf{R}_j \geqslant 5$. To validate this approach, we applied the procedure to layers within a bulk liquid system and found that $D_{j,\parallel}$ was equal to D_0, as required. The diffusion coefficient parallel to the surface for the first ten layers near the more-wetting and less-wetting solid surfaces is presented in Fig. 5(a).

3. Diffusion perpendicular to the surface

As indicated in Eq. (5), we predict the parallel-to-surface diffusion coefficient by scaling the planar MSD of atoms that remain in the layer by $P_j(\tau)$. The survival probability (which measures displacement normal to the surface) is independent of the planar MSD (which measures displacement parallel to the surface) and serves as a correction factor accounting for atoms that exit the layer. In the direction perpendicular to the surface, the MSD and survival probabilities are correlated (both measure displacement normal to the solid), and applying Eq. (5) in the z direction will bias the predicted diffusion coefficient to low values.

To predict $D_{j,\perp}$ we augment predictions from MD simulations with data from Langevin dynamics.[30] Langevin dynamics is a simulation technique that uses a stochastic dif-

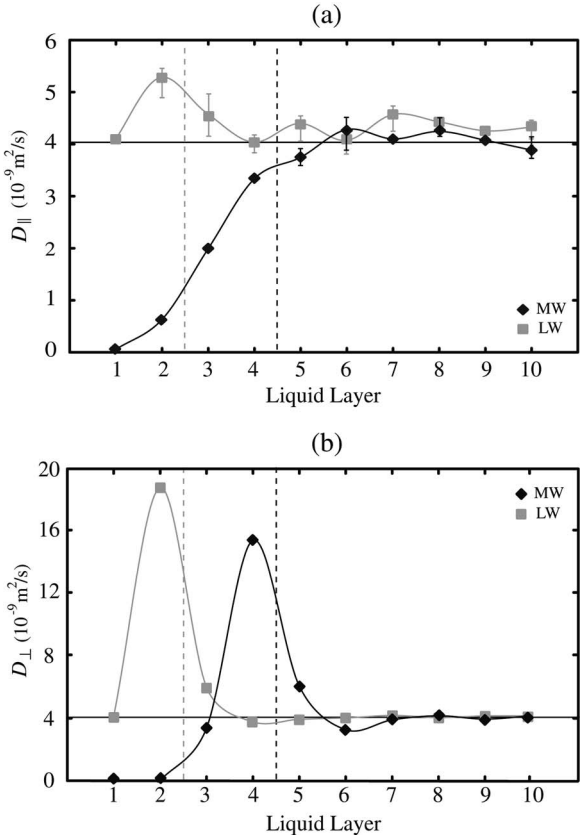

FIG. 5. (a) Diffusion coefficient parallel to the surface. (b) Diffusion coefficient perpendicular to the surface. In both plots, the solid guidelines are added to emphasize critical points and the dashed lines identify the boundary between the solid-moderated and liquid-moderated regions. The error bars represent the range of data predicted from the four data sets. Note that $D_{\parallel}$ and $D_{\perp}$ converge to D_0 (solid horizontal line) in the layers closest to the channel centerline.

ferential equation to approximate the effects of interatomic forces and random thermal motions on atomic dynamics. Although simple Langevin dynamics include neither hydrodynamic coupling nor memory effects, survival probability curves predicted from MD simulation can be reproduced by proper selection of the diffusion coefficient.[27,29]

In the direction perpendicular to the solid, the Langevin equation takes the form

$$m\ddot{z} = -\frac{k_B T}{D_z}\dot{z} + R(t) - \frac{\partial W(z)}{\partial z}, \tag{7}$$

where k_B is the Boltzmann constant, T is the system temperature, $D_z = D_{\perp}$ is a user-defined diffusion coefficient, $R(t)$ is a stochastic random force, and $W(z)$ is the potential of mean force (PMF). Unlike MD simulations, which assume that particles interact according to classical force fields, the atomic interactions in a Langevin dynamics simulation are modeled as stochastic processes governed by the fluctuation-dissipation theorem through $R(t)$.[30] Thus, while particles in a MD simulation follow deterministic position and momentum trajectories, those in a Langevin dynamics simulation follow non-time-reversible trajectories.

The layer-specific PMF is given by

$$W_j = -k_B T \ln\left(\frac{\rho_j}{\rho_0}\right). \tag{8}$$

The spatial derivative of the PMF provides a measure of the local density gradient and is obtained by interpolating the density profiles presented in Fig. 3. We perform this interpolation using a shape-preserving piecewise cubic Hermite interpolating polynomial, which ensures that the derivative is zero at all minima and maxima of the discrete data.[31]

The Langevin dynamics survival curves for each layer are generated using the following procedure.[29] A single atom is assigned a random position in a layer of width 0.785σ (corresponding to the width of the MD liquid layers). The atom is then given an initial velocity in a random direction with a magnitude equal to the average velocity predicted from the MD simulations. At each time step, a random force $R(t)$ with

$$\langle R(t)\rangle = 0 \quad \text{and} \quad \langle R(t)R(t')\rangle = \frac{6k_B^2 T^2}{D_z}\delta_{tt'}$$

is applied to the atom in a random direction. Using $R(t)$, the MD-predicted W_j, and a user-defined D_z, Eq. (7) is solved at each time step to calculate the position of the atom over a 5000 time step (21 ps) trial. When the atom is in the layer, the atom-specific survival probability at that time step is 1. If the atom leaves the layer at some point in the trial, the survival probability for the remaining time steps is zero. The atom-specific survival curves from 50 000 independent trials are averaged to form a smooth layer-specific Langevin dynamics survival curve $P_{LD}(\tau)$, which can be compared to the survival curve predicted from the MD trials. From a conceptual standpoint, layers with a high D_z are characterized by quickly decaying survival curves (i.e., a lower τ_j, as discussed in Sec. III).

The inertial effects (i.e., velocity autocorrelation) present in MD simulations lead to faster translational motions than those predicted using simple Langevin dynamics simulation.[27] This fact means that the layers used to partition the liquid and generate survival curves from the Langevin dynamics simulation may need to be narrower than those used to partition the MD liquid. Furthermore, any comparisons between the two simulation techniques should only be made after the atomic MSD measured from the MD simulation becomes linear.

The D_z term in Eq. (7) for a given layer is adjusted until the difference between $P_{LD}(\tau=9.6\text{ ps})$ and $P(\tau=9.6\text{ ps})$ is less than 0.005.[29] Once this condition is satisfied, a second comparison is made between $P_{LD}(\tau=16.8\text{ ps})$ and $P(\tau=16.8\text{ ps})$. If this second comparison yields a difference greater than 0.005, the width of the Langevin dynamics simulation layer is reduced and D_z is reevaluated. Upon obtaining suitable agreement at times of 9.6 and 16.8 ps, D_z is recorded as $D_{\perp}$ and the comparison sequence is repeated for the next liquid layer. The exact choice of comparison times, provided they are greater than 0.21 ps (the linear-quadratic transition time presented in Sec. II), was found to have little effect on the value of D_z that generated the best fit to the MD data. The predicted diffusion

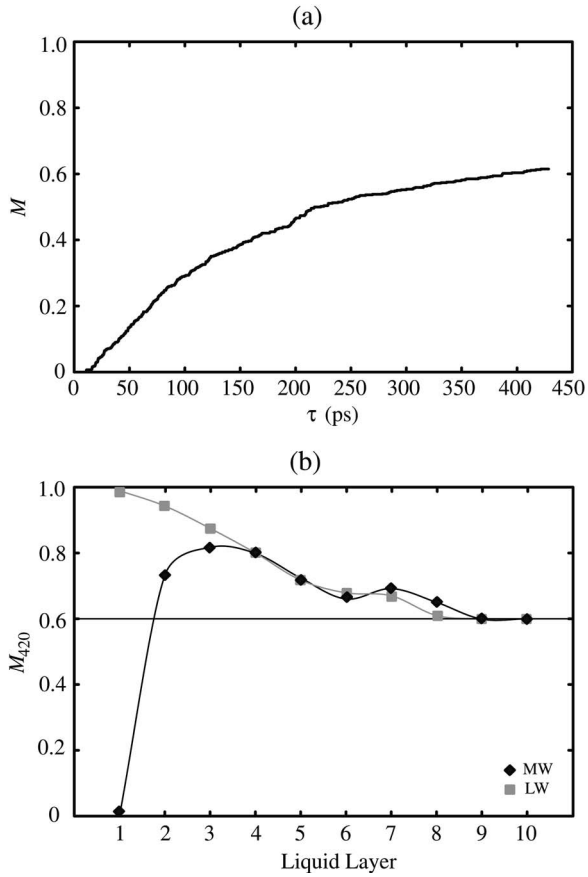

FIG. 6. (a) Time evolution of M for atoms migrating across four bulk liquid layers. (b) Atomic migration across four liquid layers in the direction away from the solid-liquid boundary. The migration fraction M_{420} identifies the fraction of atoms successfully migrating from the origin layer (layer number) to the destination layer (layer number +4) over 420 ps trials. The horizontal line identifies M_{420} for a layer in bulk liquid.

coefficient perpendicular to the surface for the first ten layers near the more-wetting and less-wetting solid surfaces is presented in Fig. 5(b).

E. Atomic migration

As introduced in Sec. II, we use the term atomic migration to describe the aggregate movement of atoms over long times across multiple liquid layers. We generate migration statistics by identifying the atoms within an origin layer, tracking their positions as they diffuse through the system, and recording the time each atom arrives at a specified destination layer. Instead of capturing local liquid dynamics, migratory statistics predict the integrated effect of spatially varying properties on atomic mass transfer.

Random interatomic collisions and varied atomic velocities reduce the probability that all atoms from the origin layer will simultaneously arrive at the destination layer. Instead, the fraction of atoms successfully migrating, M, from an origin layer to a destination layer is a function of time [i.e., $M=M(\tau)$]. As presented in Fig. 6(a), which presents $M(\tau)$ for atoms migrating across four bulk liquid layers, $M(\tau)$ monotonically increases from zero. The shape of $M(\tau)$ results from the number of diffusion paths available to migrating atoms. Some atoms may exit the origin layer and follow a direct path to the destination layer with few collisions or interactions. Other atoms may take less direct paths or cross the intermediate layers many times in the tracking period. Although all atoms from the origin layer will eventually reach the destination layer, the long trials required to observe such completion are computationally impractical. Over the 420 ps trials used here, 60% of atoms successfully migrate across four bulk layers, a fraction sufficient to resolve relevant trends.

To investigate the effects of the solid surface on liquid migration, we measure the ability of atoms originating near the surface to migrate across four liquid layers in the direction towards the channel centerline. As presented in Fig. 6(b), the fraction of atoms successfully migrating over a 420 ps trial, M_{420}, from layer j (the origin layer) to layer $(j+4)$ (the destination layer) is a function of both original distance from the solid and surface wettability. These migration data were obtained by averaging between both solid-liquid boundaries over ten independent trials. As expected, for bulklike origin layers far from the surface, M_{420} approaches the bulk value.

IV. ANALYSIS AND INTERPRETATION

A. Density and structure

The atoms in the liquid layer closest to the more-wetting surface (layer 1) assume a density and structure closely resembling the solid walls. These layer 1 atoms do not diffuse and have equilibrium positions mimicking the fcc lattice. Across layers 2–4, the movement and structure of the liquid atoms become increasingly random and, as presented in Fig. 4, the structure factor decreases monotonically to its bulk value. As shown in Fig. 3, the liquid density decreases in the direction away from the solid, reaching a minimum of $0.87\rho_0$ in layer 4, then settles to ρ_0 by layer 8. The density minimum present in layer 4 is explained as follows. In layers 1–3 near the more-wetting solid, strong attractive forces draw liquid atoms towards the solid, increasing the local liquid density. The attractive force that the solid atoms exert on the liquid atoms decreases with distance, and in liquid layers beyond the influence of the solid, the liquid atoms are repelled by the dense assembly of liquid atoms near the surface. In the current configuration, this repulsion generates a region of low liquid density in layer 4.

In the less-wetting system, the liquid-liquid interactions are stronger than the solid-liquid interactions. Thus, rather than experiencing a strong attraction towards the solid, liquid atoms are drawn towards other liquid atoms and away from the surface. This behavior generates the density profile presented in Fig. 3, in which the density increases monotonically from $0.63\rho_0$ to ρ_0 in the direction towards the channel centerline. Although the structure factor in the first two liquid layers is above the bulk value, all liquid atoms readily diffuse.

B. Diffusion within the layers

1. Diffusion perpendicular to the surface

Spatially varying anisotropic diffusion coefficient tensors have been predicted in MD simulations of liquid-vapor

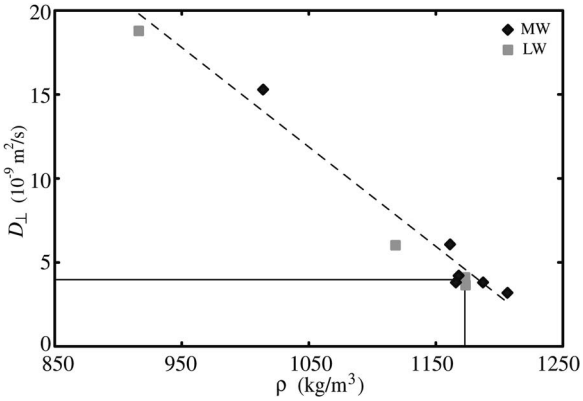

FIG. 7. Correlation between $D_\perp$ and density in liquid-moderated regions near more- and less-wetting solids. A best-fit line is added to highlight the trend. Included are data from the last layer of the solid-moderation region; these transition layers assume characteristics of both regions. The solid horizontal and vertical lines identify D_0 and ρ_0. The intersection of these two lines corresponds to bulk conditions.

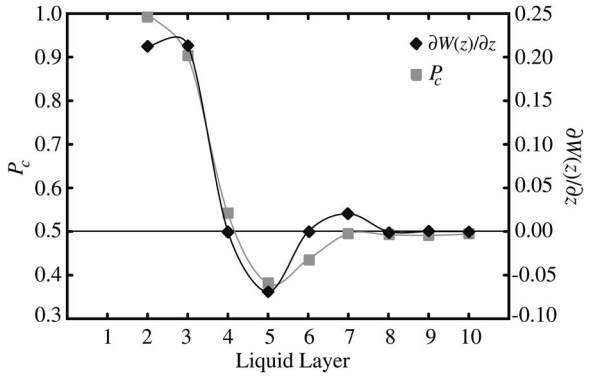

FIG. 8. Correlation between the centerline-side exit probability P_c and the derivative of the PMF for the more-wetting solid. The horizontal line at P_c=0.5 corresponds to bulklike layers where $\partial W(z)/\partial z$=0 and movement is unbiased.

water interfaces.[27,29] Wick and Dang[29] explain this behavior using a vacancy model where diffusion is enhanced in regions of low density. As presented in Figs. 5(a) and 5(b), spatially varying diffusion coefficients exist near the LJ solid-liquid boundary. In agreement with the vacancy model, and as presented in Fig. 7, $D_\perp$ is correlated to density in the liquid-moderated regions in both the more- and less-wetting simulations. Although a similar correlation between $D_\parallel$ and density likely exists, the uncertainty in our data [see Fig. 5(a)] is too great to make a definite conclusion.

The linear correlation between $D_\perp$ and density does not persist into the the solid-moderated region (not present in liquid-vapor interface systems). This is because the atomic dynamics within these regions are also affected by direct solid-liquid interactions. Thus, although liquid density variations will partially affect atomic mobility, mass transfer within the solid-moderated regions is impeded by the attractive force pulling liquid atoms towards the surface. This argument is consistent with our predictions. For example, layers 3 and 5 in the more-wetting simulation have similar densities, but $D_\perp$ in layer 3 (a solid-moderated layer) is significantly lower than $D_\perp$ in layer 5 (a liquid-moderated layer). Similarly, while the density in layer 1 near the less-wetting system is only $0.63\rho_0$, $D_\perp$ is comparable to D_0.

In the outermost solid-moderated layer (layer 4 in the more-wetting simulation and layer 2 in the less-wetting simulation), the solid-liquid interaction force is weak and $D_\perp$ becomes correlated to density (see Fig. 7). While this transition to density-moderated diffusion is expected, the $D_\perp$ maxima (see Fig. 5) are surprising. The underlying physics causing this behavior are not yet clear. However, we expect that the liquid atoms in this region have long velocity autocorrelations perpendicular to the surface, causing rapid movement into either the solid-moderated region or the liquid-moderated region.

Although governed by different mechanisms, liquid diffusion in both the solid- and liquid-moderated regions can be further understood by considering the layer-specific exit probabilities (see Sec. III) and the local liquid density gradient (as predicted by the PMF). Observe in Fig. 8 that a strong correlation exists between the centerline-side exit probability P_c and the derivative of the PMF $[\partial W_j(z)/\partial z]$ used in the Langevin dynamics simulations. When a layer has a positive $\partial W(z)_j/\partial z$, implying that the local density is decreasing in the direction of the centerline, the atoms in that layer are likely to exit away from the solid surface (i.e., $P_c > P_s$). Conversely, when $\partial W(z)/\partial z$ is negative, meaning the local atom density is decreasing in the direction of the solid, atoms in the layer are likely to exit towards the solid surface (i.e., $P_s > P_c$). Thus, although atoms in layers with enhanced $D_\perp$ more readily diffuse perpendicular to the solid, the local PMF and associated density gradient dictate the direction these atoms are likely to travel.

2. Diffusion parallel to the surface

As discussed above, $D_\parallel$ deviates from $D_\perp$ near a liquid-vapor water interface.[27,29] Liu *et al.*[27] qualitatively attribute the anisotropic mass transfer to variations in liquid structure that naturally arise near a boundary. As presented in Fig. 9, $D_\parallel$ deviates from $D_\perp$ in our solid-liquid simulations. And, in agreement with the argument presented by Liu *et al.*, this behavior is related to variations in liquid structure. Observe in Fig. 10 that a strong correlation between $D_\parallel$ and $\langle S^2(\boldsymbol{\kappa})\rangle$ is

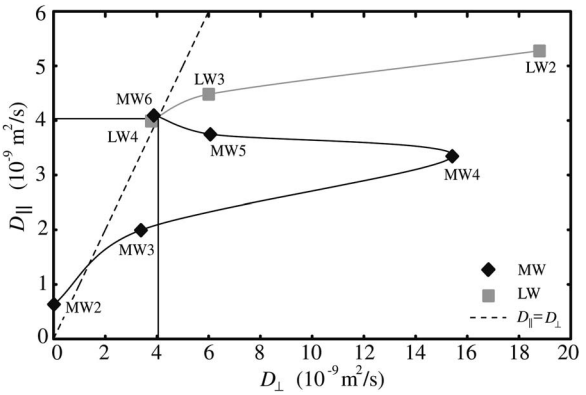

FIG. 9. Anisotropy of the diffusion coefficient tensor near the more- and less-wetting surfaces. In most layers, $D_\perp$ is greater than $D_\parallel$, implying that diffusion perpendicular to the surface is enhanced more than diffusion parallel to the surface. The dashed line represents isotropic diffusion. The solid lines correspond to D_0 of the bulk liquid.

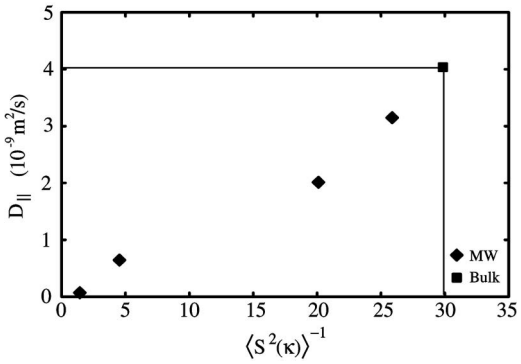

FIG. 10. Correlation between $D_{\|}$ and $\langle S^2(\boldsymbol{\kappa})\rangle^{-1}$ for liquid layers 1–4 near the more-wetting solid. Although enhanced ordering exists within layer 1 near the less-wetting surface, the low liquid density limits the impact of the liquid structure on $D_{\|}$. The horizontal and vertical lines correspond to bulk D_0 and the bulk $\langle S^2(\boldsymbol{\kappa})\rangle^{-1}$. The intersection identifies bulk conditions.

present near the more-wetting surface. This trend is expected: when $\langle S^2(\boldsymbol{\kappa})\rangle$ is high, the dense, crystal-like structure present in these layers should reduce the planar mobility of the liquid atoms. Since the magnitude of the liquid structure factor (which governs $D_{\|}$), the strength of the direct solid-liquid interactions, and the density (which governs $D_{\perp}$) are not strongly coupled, an anisotropic diffusion coefficient tensor is generated within the solid-moderated region. The differences between $D_{\|}$ and $D_{\perp}$ continue into the first liquid-moderated layer. Although direct solid-liquid interactions are negligible at this position, the lingering effects of liquid structure may damp diffusion parallel to the surface and generate the continued anisotropy.

C. Migration across the layers

As discussed in Sec. III, liquid atoms in a bulk system diffuse without directional bias, and the fraction of atoms that successfully migrate across four layers during a 420 ps trial, M_{420}, is 0.60. Because liquid atoms cannot diffuse into the solid surface, migration of liquid atoms near the solid-liquid boundary is naturally biased towards the channel centerline. Thus, as presented in Fig. 6(b), M_{420} for atoms originating near either the more-or less-wetting surface is greater than the bulk value.

Although both solids bias migration towards the channel centerline, M_{420} is a function of distance from the solid and surface wettability. Near the less-wetting solid, the layer densities are low and the solid-liquid interactions pulling atoms towards the surface are weak compared to the liquid-liquid interactions pulling atoms towards the bulk liquid. The result is a high M_{420} in layers 1 and 2 with nearly 100% of the atoms successfully migrating four layers towards the channel centerline. The increasing density (which raises the atomic collision frequency) and the growing number of diffusion paths available to atoms originating in layers 3–6 causes M_{420} to decrease monotonically to the bulk value.

As discussed, atoms in layer 1 near the more-wetting solid do not diffuse and M_{420} is zero. Across layers 2 and 3, the average solid-liquid interaction force becomes smaller while the density gradient $\partial W(z)/\partial z$ decreases in the direction away from the solid surface. These trends enhance migration towards the channel centerline and cause M_{420} to obtain a local maxima in layer 3. Across layers 4–6, the density increases in the direction towards the channel centerline, impeding migration away from the solid. Furthermore, the increased number of diffusion paths available to atoms originating within these layers cause M_{420} to decrease and to obtain a local minimum in layer 6. In layers 7 and beyond, $\partial W(z)/\partial z$ again becomes positive (meaning migration towards the channel centerline is encouraged) and M_{420} decays to the bulk value.

V. SUMMARY AND DISCUSSION

We have investigated the effect of surface wettability on liquid structure, mobility, and diffusion near a solid surface using molecular dynamics simulations. As presented in Figs. 3 and 4, the density and structure of a liquid near a solid are dependent on the surface wettability. Near the more-wetting surface, both the liquid structure factor and density are well above bulk liquid values. Near the less-wetting surface, the liquid assumes enhanced structure but the density is low. The structure factor profiles suggest a natural division between a liquid region that is moderated by solid-liquid interactions and a liquid region that is moderated by liquid-liquid interactions.

Using a modified mean-squared displacement relation and Langevin dynamics simulations, we predicted the diffusion coefficient tensor near both surfaces. The diffusion coefficient tensor, which describes diffusion parallel [Fig. 5(a)] and perpendicular [Fig. 5(b)] to the solid-liquid boundary, is spatially varying and is a strong function of surface wettability. In the liquid-moderated regions in both more- and less-wetting simulations, where solid-liquid interactions are negligible, a correlation between density and $D_{\perp}$ exists (see Fig. 7). This trend agrees with predictions from other simulations of liquid-vapor interfaces.[27,29] As presented in Fig. 10, a correlation between $D_{\|}$ and liquid structure is present in layers near the more-wetting solid. This trend between $D_{\|}$ and structure, also predicted in previous simulations of the liquid-vapor interface,[27,29] seems sensible; the enhanced ordering in these layers should reduce the planar mobility of the liquid atoms. Because $D_{\|}$ and $D_{\perp}$ are governed by different phenomena, an anisotropic diffusion coefficient tensor is generated near the surface. As seen in Fig. 9, the directional dependence of the diffusion coefficients (represented as the ratio of $D_{\|}$ to $D_{\perp}$) is a function of surface wettability.

We also investigated the effects of surface wettability on atomic migration, the diffusion of atoms across many liquid layers. As presented in Fig. 6, the fraction of atoms successfully migrating from an origin layer to a destination layer is a function of time. The shape of this curve results from the variety of diffusion paths available to migrating atoms. Over a certain tracking period, the fraction of liquid atoms successfully migrating away from the solid surface is a function of surface wettability and distance from the solid. Observe in Fig. 6(b) that atoms near a solid of either wettability are likely to diffuse towards the channel centerline. However, due to significant solid-liquid interactions, liquid atoms near

the more-wetting solid are less likely to migrate towards the centerline compared to atoms near the less-wetting surface.

The presence of an anisotropic diffusion tensor and the effects of surface wettability on atomic migration may be used to generate tailored mass transport properties. For example, tuning the surface wettability of the channel walls in diffusion-limited micro- and nanofluidic reactions may be one way to obtain desired reaction rates. Similarly, the surface wettability could be altered to ensure that targets quickly migrate towards certain functional surfaces while other targets, on account of the anisotropic diffusion coefficient tensor, are led to alternative reaction sites.

In molecular liquids, such as water and organic solvents, ordering and density variations are further enhanced by hydrogen bonding and electrostatic forces.[32] In preliminary investigations, such interactions have been shown to generate a spatially varying anisotropic diffusion coefficient tensor.[8] However, a high spatial resolution, mechanistic investigation into the transport properties (diffusion coefficient, viscosity, and thermal conductivity tensor) of liquid water near a solid surface must still be performed.

[1] J. Berthier and P. Silberzan, *Microfluids for Biotechnology* (Artech House, Boston, 2006).
[2] M. Wortis, *Ordering in Two Dimensions* (North Holland, New York, 1980).
[3] R. F. Hainsey, R. Gangwar, J. D. Shindler, and R. M. Suter, Phys. Rev. B **44**, 3365 (1991).
[4] G. Arya, H.-C. Chang, and E. J. Maginn, Mol. Simul. **29**, 697 (2003).
[5] J.-L. Barrat and F. Chiaruttini, Mol. Phys. **101**, 1605 (2003).
[6] A. R. Abramson, C.-L. Tien, and A. Majumdar, J. Heat Transfer **124**, 963 (2002).
[7] M. Angadi, T. Watanabe, A. Bodapati, X. Xiao, O. Auciello, J. A. Carlisle, J. A. Eastman, P. Keblinski, P. K. Schelling, and S. R. Phillpot, J. Appl. Phys. **99**, 114301 (2006).
[8] S. H. Lee and P. J. Rossky, J. Chem. Phys. **100**, 3334 (1994).
[9] M. Cieplak, J. Koplik, and J. R. Banavar, Phys. Rev. Lett. **86**, 803 (2001).
[10] C.-J. Yu, A. G. Richter, J. Kmetko, S. W. Dugan, A. Datta, and P. Dutta, Phys. Rev. E **63**, 021205 (2001).
[11] L. P. Faucheux and A. J. Libchaber, Phys. Rev. E **49**, 5158 (1994).
[12] S. Maruyama, T. Kurashige, S. Matsumoto, Y. Yamaguchi, and T. Kimura, Microscale Thermophys. Eng. **2**, 49 (1998).
[13] S. C. Hendy, M. Jasperse, and J. Burnell, Phys. Rev. E **72**, 016303 (2005).
[14] O. Kuksenok, J. M. Yeomans, and A. C. Balazs, Phys. Rev. E **65**, 031502 (2002).
[15] O. Kuksenok and A. Balazs, Phys. Rev. E **68**, 011502 (2003).
[16] A. J. H. McGaughey, M. I. Hussein, E. S. Landry, M. Kaviany, and G. M. Hulbert, Phys. Rev. B **74**, 104304 (2006).
[17] A. I. Skoulidas and D. S. Sholl, J. Phys. Chem. B **105**, 3151 (2001).
[18] D. Bedrov and G. D. Smith, J. Chem. Phys. **113**, 8080 (2000).
[19] K. Meier, A. Laesecke, and S. Kabelac, J. Chem. Phys. **121**, 9526 (2004).
[20] P. Keblinski and J. Thomin, Phys. Rev. E **73**, 010502(R) (2006).
[21] L. Xue, P. Keblinski, S. R. Phillpot, S. U.-S. Choi, and J. A. Eastman, Int. J. Heat Mass Transfer **47**, 4277 (2004).
[22] N. W. Ashcroft and N. D. Mermin, *Solid State Physics* (Saunders College, Fort Worth, 1976).
[23] B. J. Berne and G. D. Harp, Adv. Chem. Phys. **17**, 63 (1970).
[24] D. A. McQuarrie, *Statisitcal Mechanics* (Viva Books, New Delhi, 2005).
[25] A. Rahman, Phys. Rev. **136**, A405 (1964).
[26] J. F. Lutsko, D. Wolf, S. R. Phillpot, and S. Yip, Phys. Rev. B **40**, 2841 (1989).
[27] P. Liu, E. Harder, and B. J. Berne, J. Phys. Chem. B **108**, 6595 (2004).
[28] R. Zwanzig, Annu. Rev. Phys. Chem. **16**, 67 (1965).
[29] C. D. Wick and L. X. Dang, J. Phys. Chem. B **109**, 15574 (2005).
[30] M. P. Allen and D. J. Tildesley, *Computer Simulation of Liquids* (Oxford University Press, New York, 1987).
[31] C. Moler, *Numerical Computing with Matlab* (Society for Industrial and Applied Mathematics, Philadelphia, 2004).
[32] L. Cheng, P. Fenter, K. L. Nagy, M. L. Schlegel, and N. C. Sturchio, Phys. Rev. Lett. **87**, 156103 (2001).